



Batnikov, A.S., Kusyumov, A.N., Mikhailov, S.A. and Barakos, G.N. (2018) Aerodynamic optimization of helicopter rear fuselage. *Aerospace Science and Technology*, 77, pp. 704-712. (doi: [10.1016/j.ast.2018.03.046](https://doi.org/10.1016/j.ast.2018.03.046))

This is the author's final accepted version.

There may be differences between this version and the published version. You are advised to consult the publisher's version if you wish to cite from it.

<http://eprints.gla.ac.uk/159846/>

Deposited on: 30 March 2018

Enlighten – Research publications by members of the University of Glasgow  
<http://eprints.gla.ac.uk>

# Aerodynamic Optimization of Helicopter Rear Fuselage

A. S. Batrakov<sup>1</sup>, A. N. Kusyumov<sup>2</sup> and S. A. Mikhailov<sup>3</sup>  
*KNRTU-KAI, Kazan, Russia*

G. N. Barakos<sup>4</sup>  
*Glasgow University, Glasgow, UK*

**An optimization process for the rear helicopter fuselage part is presented using Genetic Algorithms and Kriging surrogate models. Shape parameterization is carried out with the super ellipse technique employed for the well-known ROBIN fuselage. The simulations were based on the RANS equations solved using the HMB CFD code. It is shown that a decrease of fuselage drag around 2.5% is possible without compromising the structure and the functionality of the design. Combined with an optimization of the helicopter skids, benefits of up to 4.6% were possible. The demonstrated method can be applied to fuselages of any shape during the initial design phase.**

## Nomenclature

$x_0, y_0, z_0$	=	origin of super-ellipse center
$A, B$	=	length and width of the super-ellipse
$N$	=	power of curve
$x, y, z$	=	Cartesian coordinates
$r, \varphi$	=	polar coordinates
$CD$	=	drag coefficient
$M$	=	Mach number
$Re$	=	Reynolds number

## Keywords

Aerodynamics, Helicopter fuselage, Optimization, Genetic Algorithm, Kriging model

---

<sup>1</sup> Researcher, Laboratory №1 of KNRTU-KAI, Russia, Kazan, K. Marks street, 10, Batrakov\_a.c@mail.ru

<sup>2</sup> Professor, Laboratory №1 of KNRTU-KAI, Russia, Kazan, K. Marks street, 10, Postbox7@mail.ru

<sup>3</sup> Professor, Laboratory №1 of KNRTU-KAI, Russia, Kazan, K. Marks street, 10, sergey.mikhaylov@kai.ru

<sup>4</sup> Professor, Glasgow University, Glasgow, UK, George.Barakos@glasgow.ac.uk

## 1. Introduction

The design of a helicopter fuselage is a difficult and complex task with compromises between structural and aerodynamic requirements. Most of the times, engineers are looking for small changes in geometry and structure to improve an already good design. Past and recent studies (for isolated fuselages and full helicopter models) show that a significant contributor to the total drag of the helicopter fuselage is suction at its rear due to aft-facing surfaces used for ramps and rear-access [1-15].

This is the reason for streamlined helicopter fuselage shapes. An example is the Sikorsky UH-60A helicopter with a smooth aft-facing surface at the fuselage tail-boom junction area. In contrast to this trend there are helicopters with a salient area of fuselage/tail-boom junction. Examples include the Bell 206, BK 117, and the EC 135.

This high drag region (at the fuselage/tail boom junction area) is also characterized by the presence of a vortical flow. It is known [1] that two types of vortical structures can be found at this separated flow region: eddies, that run across the flow close to the fuselage/tail boom junction area, and vortex pairs, located symmetrically to the mid-plane of the helicopter and are aligned with the free stream flow direction. Numerical simulation of these structures behind an isolated helicopter fuselage was presented by Batrakov et al. [11].

One of the ideas for improving the fuselage aerodynamic characteristics is to change these vortical structures. This can be achieved in many ways including active flow control by flow suction and blowing [4], passive flow control using devices like vortex generators [5, 16], and shape optimization [6].

Active flow control at the rear of a helicopter fuselage was investigated by Lineard et al. [4] and also in Refs. [17-21]. Investigations were carried out using experiments, as well as, numerical simulation. The active flow control was realized by blowing (steady and pulsed), and results show that the fuselage drag can be reduced by up to 10-35%. The drag reduction depends on the type of actuators and their parameters, like blowing flow ratio etc. The disadvantage of this active approach is the necessity to install additional equipment that requires additional power.

An alternative approach is based on changing the fuselage geometry. Different fuselage shapes and landing skids were investigated by Schneider et al. [21] and Reiß et al. [22]. New geometries were constructed, and results of these investigations show good potential for reducing the fuselage drag.

Another way to reduce drag is to find the optimal shape of the helicopter fuselage. To this aim, different optimization approaches are used. Any optimization requires parameterization of the geometry, and geometries can be fully [3], or partly parameterized [6, 23, 24]. A fully parameterized geometry is a good approach for the first steps in the design of a new helicopter. Due to design constraints, however, a partial parameterization is more useful.

This work presents a framework for the minimization of helicopter fuselage drag employing CFD in conjunction with a surrogate model based on Kriging method [25], and a Genetic Algorithm (GA) optimization method. GA originated from the theory of natural evolution and is widely used as a global optimization tool [26]. An advantage of the GA is that it does not need gradient information. Therefore, GA is suitable in finding the global optimization point and design variable set. GA application for 3-D aerodynamic design problems presented for example in references [27, 28]. As an alternative approach, an adjoint based optimization method [23, 24] has also been successfully applied to aft fuselage shape optimization, resulting in an aft body, strake.

The type of employed parameterization determines the number of design parameters, and the size of the design space. For a real helicopter, it is important to improve aerodynamics by introducing small changes in the geometry that can be easily implemented, without severe implications on the strength and weight of the airframe.

## 2. Fuselage optimization case

This paper demonstrates an optimization approach for the fuselage of the prototype ANSAT helicopter, produced by the Kazan Helicopter Plant of the Russian Federation (Fig. 1). The ANSAT is a multi-purpose light helicopter with a classic single-rotor design. The main rotor consists of four blades and the tail rotor consists of two. The length of the fuselage is 11 m and the mid-ship sectional area is 4 m<sup>2</sup>, approximately. The maximum take-off weight is 3600 kg. The main characteristics of this helicopter are presented in Table 1.



**Fig.1.** The ANSAT Helicopter.

During the early stages of this investigation a wind tunnel model of the helicopter was constructed, broadly corresponding to one of the ANSAT prototypes (Fig. 2). The wind tunnel model fuselage had a length 1.8 m and a mid-ship sectional area of 0.1085 m<sup>2</sup>. A CAD model was also constructed (Fig. 3), including the fuselage, landing skids, and tail plane. During this investigation the flow around isolated fuselage parts, as well as, the complete fuselage were considered.



**Fig. 2.** Wind tunnel model.

**Table 1**

Main characteristics of the helicopter ANSAT.

Performance	
Max speed	275 km/h
Cruise speed	220 km/h
Max. flight range with main fuel tanks	515 km
Operational ceiling	4800 m
Hover ceiling (OGE)	2500 m
Weight Parameters	
Max. take-off weight	3600 kg
Max. payload in transport cabin	1234 kg
GT engines (2xPW207K)	
Take-off power	630 h.p
Contingency power	710 h.p

Cabin Dimensions	
Length	5700 mm
Width	1770 mm
Height	1370 mm
Volume	8.0 m <sup>3</sup>

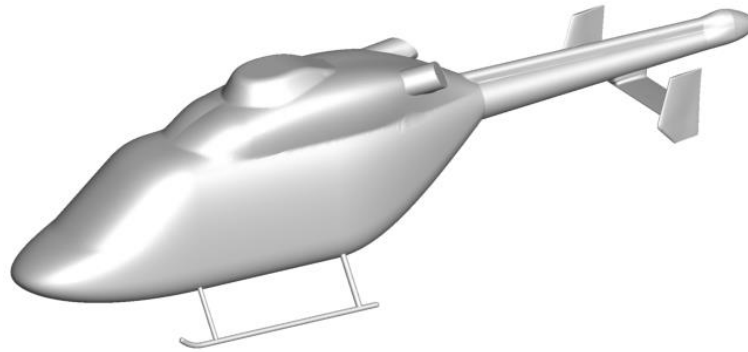


**Fig. 3.** CAD model of the ANSAT prototype.

### 3. HMB CFD Code

The simulation of the flow around the helicopter fuselage was conducted using the RANS equations with the HMB CFD code [29]. HMB uses the finite volume method and to close the RANS equations, turbulence models are used. The solver has turbulence models like the Spalart – Allmaras [30], the  $k-\omega$  [31], and the  $k-\omega$ -SST [32], as well as, hybrid approaches like DES, SAS [33], and LES. This solver employs multi-block hexa-grids, constructed using the ICEM<sup>TM</sup> Hexa tool. The HMB code has been used for investigations of the flow around the isolated helicopter fuselage [10-12], and for validation, wind tunnel tests were used.

The simulation of the flow around the isolated helicopter was carried out with  $k-\omega$  SST turbulence model in steady state mode. The baseline grid for the isolated fuselage contained 964 blocks and  $13.5 \times 10^6$  cells. An O-grid topology was used around the fuselage to resolve the surface boundary layer. The spacing of the near-wall grid in the normal to surface direction was  $1 \cdot 10^{-5}$  of the fuselage length and the employed grid resolution allows for capturing separated flow structures around the fuselage.

Results for mesh sensitivity analysis are shown in table 2. The table presents lift ( $CL$ ) and drag ( $CD$ ) coefficients for different parameters of the computational grids (including cell ratio, near-wall spacing, and grid size). At a Reynolds number of  $4.4 \times 10^6$ , and Mach of 0.1 the wind tunnel data suggest  $CL=-0.06$  and  $CD=0.09$ . Comparison of CFD and experimental data suggests that the drag coefficient values are slightly over predicted in the comparison to the experimental data. The reverse is the case for the lift coefficient. The differences between CFD and experimental results can be explained by possible errors of the positioning of the fuselage at zero pitch angles in the wind tunnel. Nevertheless, the results presented in paper [12] show similar trends as experiments. Small variations of the pitch angle lead to similar change of the aerodynamics coefficients ( $\Delta CL \approx \pm 0.014$  and  $\Delta CD \approx \mp 0.005$  for  $\Delta \alpha = 0 \pm 1$  degrees).

Using an unsteady solution did not lead to significant changes in the results of the aerodynamic characteristics of the fuselage [12]. More detailed studies about grid sensitivity and the HMB code validation vs. experimental data are presented in [10, 12, 13].

**Table 2**  
Grid parameters and fuselage aerodynamic characteristics.

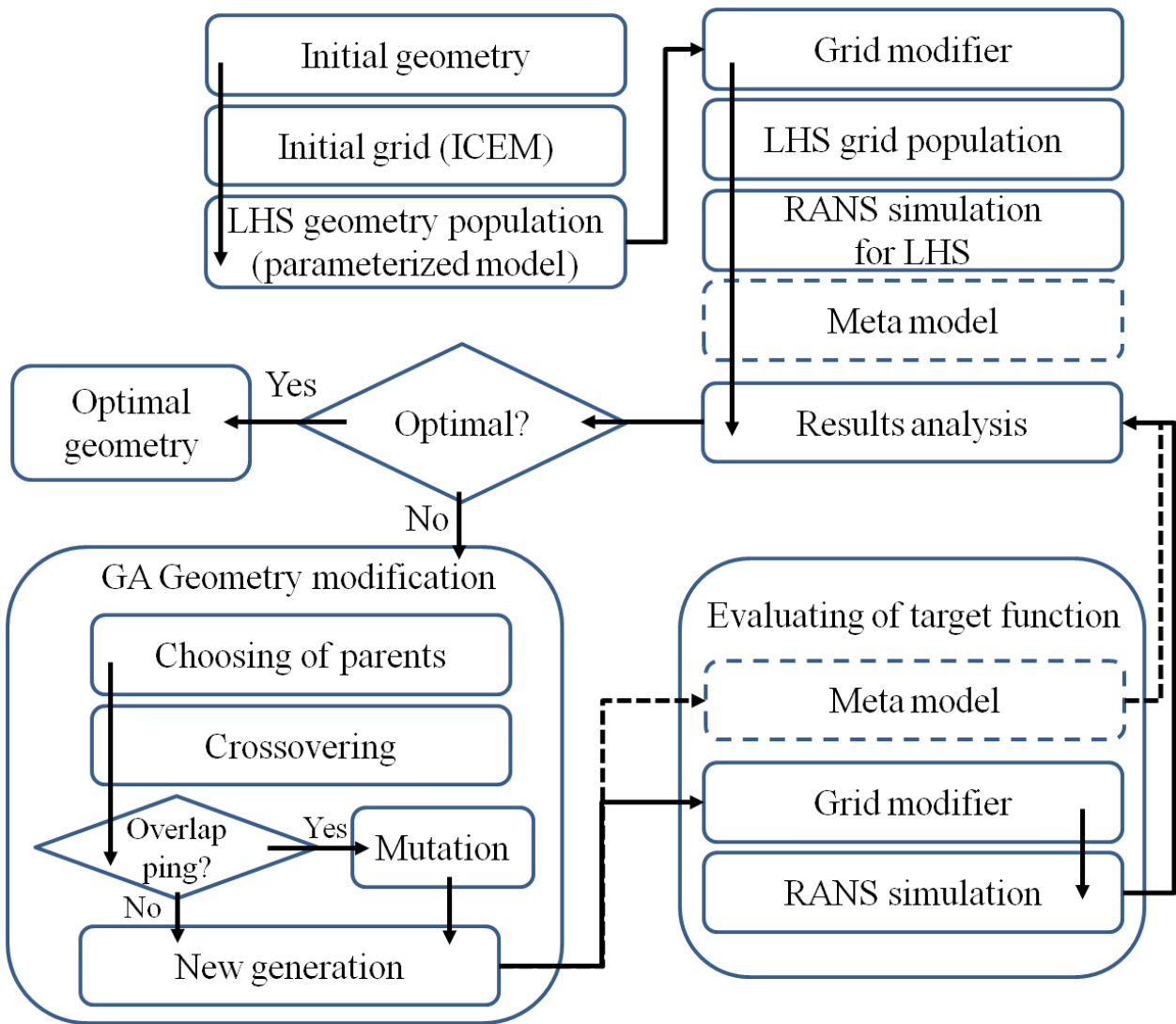
<b>№</b>	<b>Ratio</b>	<b>Spacing</b>	<b>Grid size</b>	<b>CD</b>	<b>CL</b>
1	1.3	$1 \cdot 10^{-5}$	12.5	0.098	-0.073
2	1.1	$1 \cdot 10^{-5}$	16.0	0.098	-0.074
3	1.2	$1 \cdot 10^{-5}$	13.5	0.097	-0.073
4	1.2	$2 \cdot 10^{-5}$	13.0	0.097	-0.073
5	1.2	$5 \cdot 10^{-5}$	14.0	0.098	-0.073

Table 2 data shows that the numerical simulation results (within the range of grid parameters used during the optimization process) are not affected by mesh density. Grid №2 was then used due to its low computational cost and good boundary layer resolutions.

The CFD grids used here were constructed using the same topology and design as in paper [12] where validation results for fuselage drag are also shown.

#### 4. Optimization Process

An overview of the optimization algorithm is presented in Fig. 4. Multi-block structured grids for an initial geometry were created using the ICEM<sup>TM</sup> commercial tool. After creating the parameterized model, the initial design population was defined by the Latin Hypercube Sampling method [34] (LHS) for a volume of the initial population. Then for each design variant the computational grid has adapted using a special computer program, written in C (some details of the grid modification method given in section 5). To evaluate the target function (drag coefficient) RANS simulations were used for each member of the LHS population. If the optimal result was not reached, the new generation was constructing using the GA.



**Fig. 4.** Flowchart of the optimization algorithm.

The target function evaluation method depends on the size of the employed computational grid. For low and moderate grid sizes the CFD approach can be used directly. In this case the computational grid is adapted using a special grid-modification tool and then the target function is evaluated using the RANS CFD code. Due to the high computational cost of the target function evaluation by the CFD (for big grids), a surrogate model can be used based on the Kriging [25] method. To construct the surrogate model, an initial CFD field is used, and the initial design space is narrowed using the Latin Hypercube sampling approach.

The results of each variant were normalized according to their fitness

$$C_i = \frac{1/CD_i}{\sum_{j=1}^P 1/CD_j}, \quad (2)$$

where  $CD_i$  is the drag coefficient of the each design, and  $P$  is the population size. The best part of population was selected as parents for a new generation that was produced by a crossover technique (Fig. 5(a)). For the present research, after a series of experiments the 5 best variants were selected as parents for a new generation. Recombination of the parameters was carried out at a random point. In this approach, after several iterations, a new variant may be exactly the same as one of the previously calculated ones. For more flexibility during optimization, mutations are used.

The standard approach for mutation is a random change of any design parameter. In this work an alternative pseudo-random approach was employed (Fig. 5(b)). The parameters were changed in a pseudo-random scheme with gradual shifting to the best variant from a previous step (this approach resembles a low relaxation method widely used CFD community for a differential equations discretization process). In Fig. 5(b)  $x'_n$  is one the changed parameters;  $x_n$  is the parameter before modification;  $x_{n,opt}$  is the parameter of the best variant from the previous step, and  $k$  is a random factor (in this study  $k=0\div 0.1$ ). This method of pseudo-random modification improves the convergence of the optimization process.

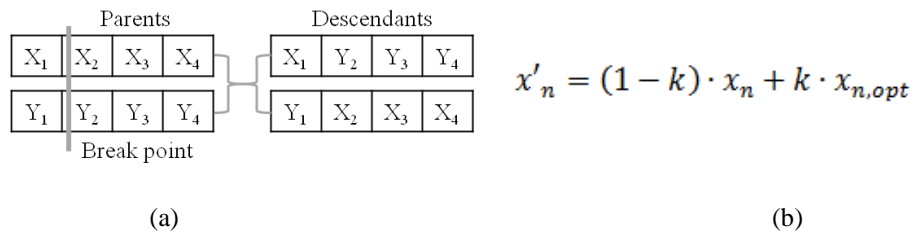


**Fig. 5.** Details of the GA: (a) Crossovering; (b) Mutation.

After the definition of a new generation, the optimization loop was closed. The process was stopped when the minimum of the drag coefficient did not change more than 1% after the 5 last generations.

For the current investigation, a mesh adaptation algorithm was developed. This algorithm allows automatic updates and calculation of the grid for new design variants. For the current investigation, shape parameterization was carried out with the super-ellipse technique employed for the well-known ROBIN fuselage [35]. This technique delivers accurate reproduction of a part of the geometry with few design parameters.

## 5. Cross Section Optimization of the Landing Skids

Optimization of the cross-section of the landing skids was considered as a test task for investigation of the GA efficiency. According to Batrakov et al. [12] for the considered helicopter model the landing skids contribute up to 20% of the total drag in some cases. Due to this reason their aerodynamic drag is high. To minimize the drag it is necessary to install a fairing over the landing skids, and the question is to find the optimal fairing geometry.

The cross section of the skids was parameterized as a super-ellipse:

$$\begin{aligned}
 y + y_0 &= r \cdot \cos \varphi \\
 x + x_0 &= r \cdot \sin \varphi
 \end{aligned} \tag{1}$$

$$r = \left[ \frac{(AB)^N}{(A \cdot \sin \varphi)^N + (B \cdot \cos \varphi)^N} \right]^{1/N}$$

The parameterizations of the leading and trailing parts were carried out separately and the details of the geometric interpretation of the components of the super-ellipse equation as applied to this task are presented in Fig. 6(a). The height of the ellipse ( $A$ ) was kept constant. The lengths ( $B_1$ ,  $B_2$ ) and the curvatures ( $N_1$ ,  $N_2$ ) of the leading and trailing parts were modified (Fig. 6(b)). Thus at the current investigation, 4 design variables were considered:  $B_1$ ,  $B_2$ ,  $N_1$ ,  $N_2$ .

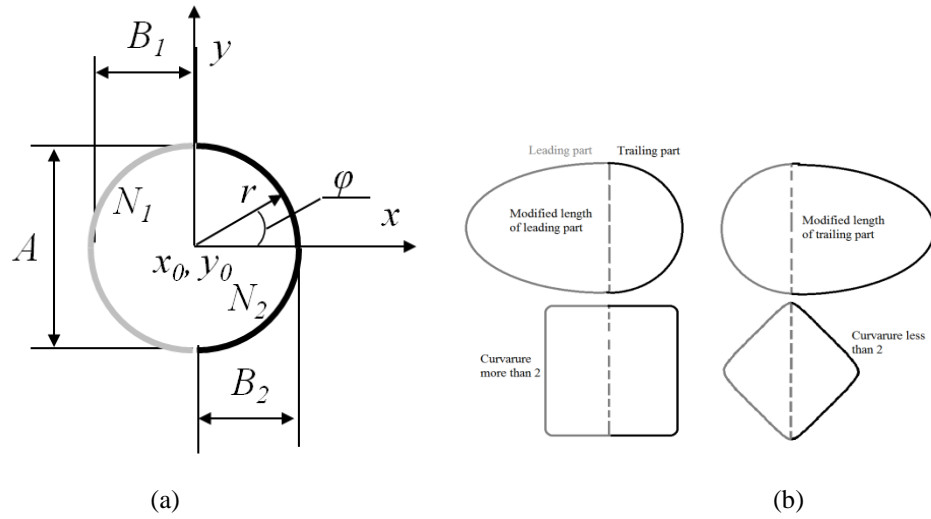


**Fig. 6.** Parameterized geometry of skid cross section: (a) Components of super-ellipse equation; (b) Modification of cross section.

To simulate the flow around the skids, a cross section was created in ICEM<sup>TM</sup> Hexa. The multi-block structure and the mesh are presented in Fig. 7. The grid consisted of 22 blocks and had O-Grid topology around the super-ellipse. This topology allows to create a grid with high resolution near and behind the skid.

The boundaries of the computational domain were placed more than 10 diameters away from the skid. The total number of grid cells was 26300, the cell height near the cross section was  $1 \cdot 10^{-6}$  of its diameter, and the expansion ratio between cells was less than 1.15.

At every design iteration, the grid was automatically updated as presented in Fig. 8.

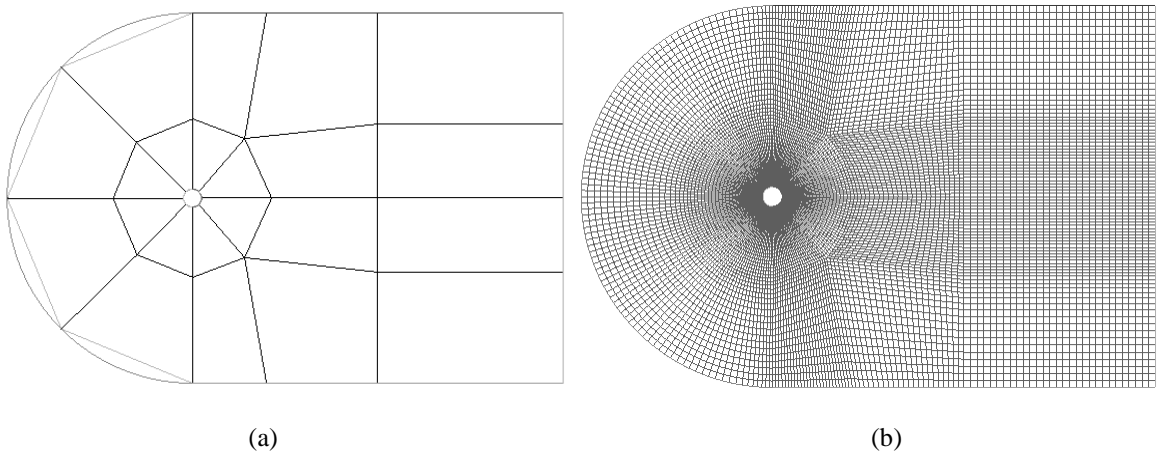


**Fig. 7.** Blocking structure (a) and grid (b) for landing fairing.

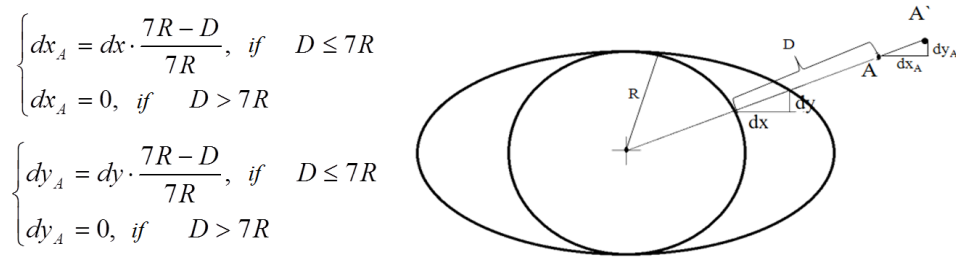


**Fig. 8.** Mesh update method.

Starting from a circular cross-section, the displacement ( $dx_A$ ,  $dy_A$ ) of any grid point (A) depends on the displacements ( $dx$ ,  $dy$ ) in the corresponding direction, and the distance ( $D$ ) between the grid point and a geometry boundary. According to this approach the grid changes in the region around the ellipse do not exceed  $7R$ . A computer code in C language was written for this specific task receiving as input the initial mesh and parameters of the geometry and producing modified grids. This approach allows for automated grid and body transformation without using the ICEM<sup>TM</sup> grid generator.

The simulation of the flow around the cross section was carried out Mach number  $M=0.1$  and Reynolds number  $Re=1 \cdot 10^5$  (based on the diameter of the initial geometry).

Taking into account that 2D calculations do not require a lot of CPU time the employed GA [36] did not use the surrogate model. A typical convergence history is presented in Fig. 9(a). The optimization process was stopped after 29 generations. Taking into account, that every generation consists of 10 samples, the total number of calculations is 290. As a result of this investigation the parameters of the optimal fairing cross section were obtained. The optimal geometry looks like a symmetric airfoil with thickness of 38.835%C. In Fig. 9(b), the aerodynamically improved cross section is presented in comparison with a NACA 0039 aerofoil.

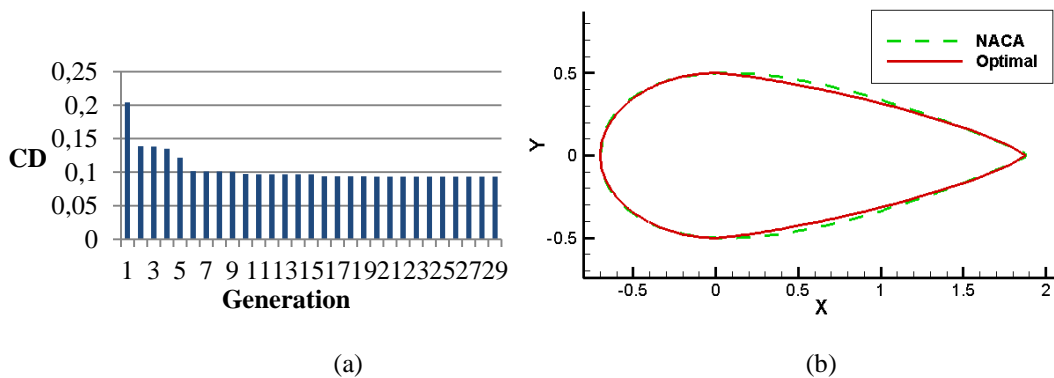


**Fig. 9.** Results of optimization process: (a) Convergence history; (b) Aerodynamically improved cross section.

## 6. Fuselage Optimization

The GA and the grid reconstruction approach of section 5 were applied for the optimization of the rear fuselage. As noted earlier, the high drag coefficient of an isolated fuselage is partly due to the vortical flow behind it. For this reason, a part of the fuselage was considered for optimization as presented in Fig. 10(a). This part has a leading boundary near the midline cross section, and a trailing boundary near the tail boom root. A geometric interpretation of the employed super ellipse parameters is presented in Fig. 10(b). The parameterized fuselage was based on a modified super ellipse equation (Eq. 3) where the parameters are presented as polynomial functions of the  $x$  coordinate (along the fuselage). The coefficients  $y_m$ ,  $A_m$ ,  $B_m$ ,  $N_m$  were defined using a least squares method and the parameterized model has negligible differences with the initial fuselage geometry (Table 3).

**Table 3**

Coefficients of polynomial functions.

	m=1	m=2	m=3	m=4
$y_m$	3.2843	-11.956	14.069	-5.2767
$A_m$	-1.6916	6.2653	-7.1197	2.5501
$B_m$	0.2294	-1.3679	2.5477	-1.4089
$N_m$	73.113	-216.35	221.36	-76.268

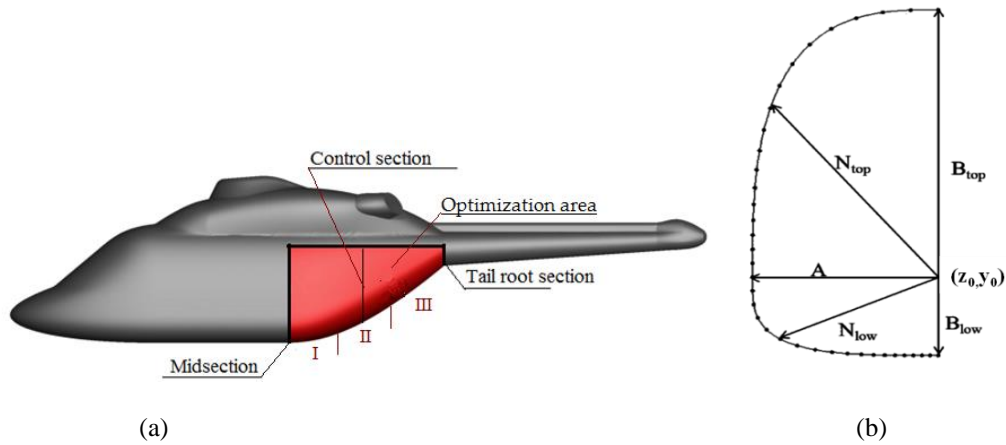


**Fig. 10.** (a) Optimization area of the isolated fuselage; (b) Parameterized model of a fuselage cross section.

$$\left\{ \begin{array}{l}
z + z_0 = r \cdot \cos(\varphi) \\
y + y_0(x) = r \cdot \sin(\varphi) \\
r = \left[ \frac{A(x) \cdot B(x)}{(A(x) \cdot \sin(\varphi))^{N(x)} + (B(x) \cdot \sin(\varphi))^{N(x)}} \right]^{\frac{1}{N(x)}} \\
y_0(x) = \sum_{m=0}^3 y_{m+1} \cdot x^m \\
A(x) = \sum_{m=0}^3 A_{m+1} \cdot x^m \\
B(x) = \sum_{m=0}^3 B_{m+1} \cdot x^m \\
N(x) = \sum_{m=0}^3 N_{m+1} \cdot x^m
\end{array} \right. \quad (3)$$

To modify the geometry it was decided to change the parameters of one cross section (termed the control section). The other sections were changed according to a sinusoidal law such that the boundaries (midsection and tail boom root) were constant. In this case, the height ( $dB$ ), the curve power ( $dN$ ), and the position of the control section ( $dX$ ) were considered as design variables. This approach allowed for changes of the tail boom and engine cowling geometry or midline section shape without any modification of assigned constraints.

Due to the high computational cost of the target function (drag coefficient) the optimization process was based on the surrogate model. To create the surrogate model Kriging was used, constructed based on 40 samples from the design domain (the CFD computation time for fuselage is about one day and the grid reconstruction process takes 15 minutes). To find the optimal design parameters, the GA was used. Results of the optimization process and the evaluation of the target function are presented in Fig. 11.

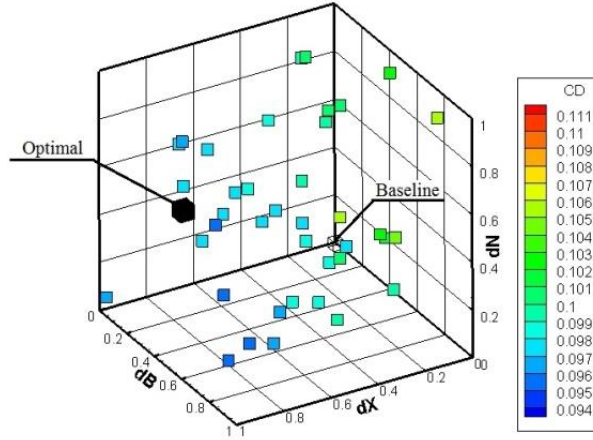


**Fig. 11.** Design domain and result of optimization.

The rear fuselage can be divided into several parts, as shown in Fig. 10. Comparison of the geometry for the initial and modified fuselages shows that the modified parts I and III underwent strong transformations, unlike the part II (close to the control section area). Thus the modified (part I) shape is more streamlined and part III is close to a bluff body shape. The modified, streamlined, part I reduced the separation area at the rear fuselage and leads to an overall increase of the pressure coefficient on the modified rear part of the fuselage (Fig. 12, 13).

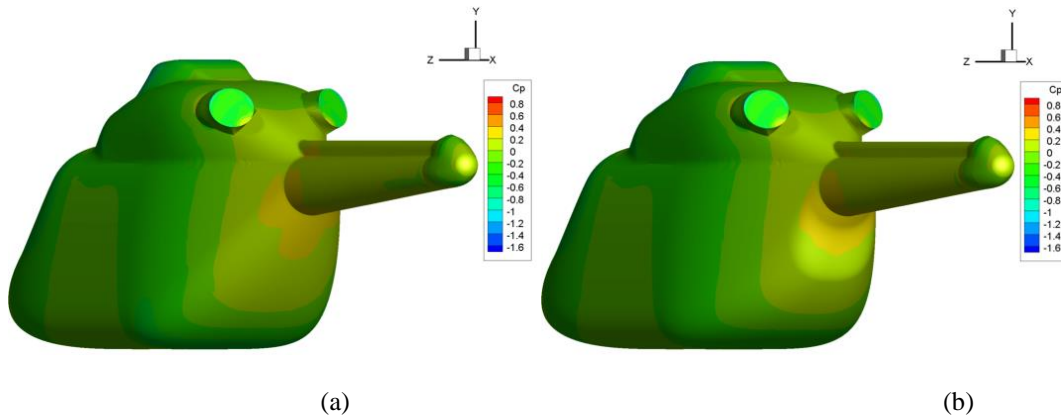


**Fig. 12.** Pressure coefficient distribution: (a) baseline; (b) modified.

Mach number  $M=0.1$ , Reynolds number  $Re=4.4 \cdot 10^6$ .

As a result of the optimization process, the parameters of the fuselage were obtained. The simulation of the flow around the modified geometry shows that the drag of the isolated helicopter fuselage decreased by up to 2.5% in comparison with the baseline geometry. It can be noted that modification of the fuselage geometry led to improvements of the lift coefficient of the isolated fuselage. The down force was reduced up to 23% ( $CL$  value for the baseline model of  $-0.072$  vs  $CL$  of  $-0.055$  for modified fuselage). It is important that this drag reduction was

achieved by small changes of the geometry (the maximum difference with the initial geometry is 16.5 cm for a full size fuselage of 11 m length). The reason behind the reduction of the aerodynamic drag is the change of the pressure distribution (Fig. 12) on the aft fuselage surface.

The surface modification leads to an overall increase of the pressure coefficient on most of the rear part of the fuselage (Fig. 13).

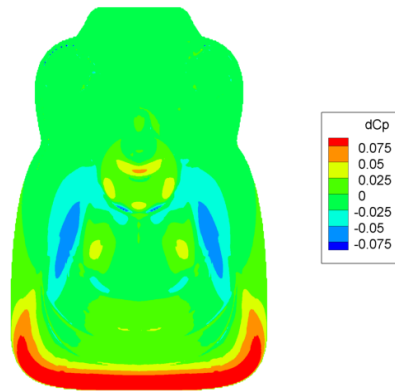


**Fig. 13.** Difference in pressure coefficient distribution between initial and optimized shapes at the rear fuselage.

## 7. Fuselage Layout

The previous section presented optimization results of an isolated fuselage. The components of the fuselage (for example landing skids) can also influence the flow and change the fuselage aerodynamic characteristics. For this reason, the flows around different fuselage configurations were considered. A more complex configuration consists of the fuselage (Fus), landing skids (LS), and tail plane (TP). The results of the drag evaluation for different layouts with the baseline and modified fuselage geometries are presented in Fig. 14.

It is shown that all configurations with the modified fuselage geometry have a lower drag coefficient. Note that the drag decrease for the fuselage with landing skids is larger than the decrease for the isolated fuselage. One of the reasons is the influence of the landing skids on the pressure distribution of the rear fuselage (Fig. 15).

The difference of the surface pressure distribution due to the shape optimization of the fuselage with landing skids on, is presented in Fig. 16, with respect to the original design.

According to the results of section 5, the landing skids were also modified by adding fairings (Fig. 17) in the fuselage configuration.

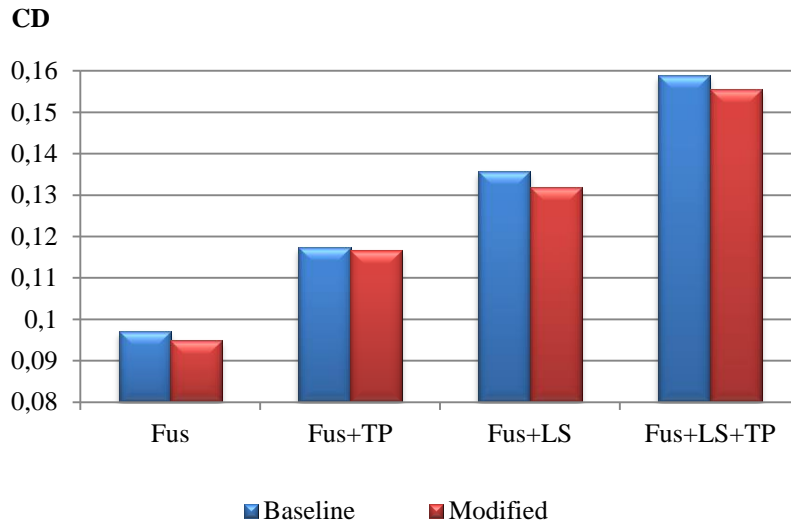


**Fig. 14.** Drag coefficient for different fuselage layouts.

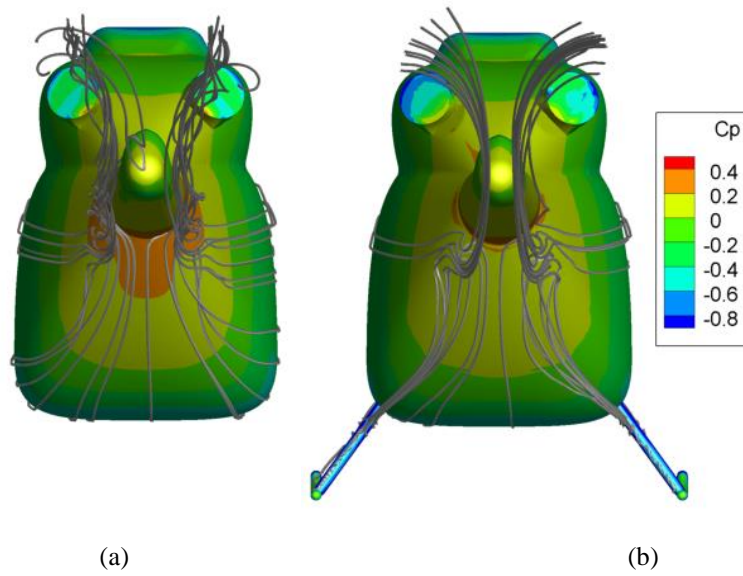


**Fig. 15.** Pressure distribution on the isolated fuselage (a) and fuselage with landing skids (b)

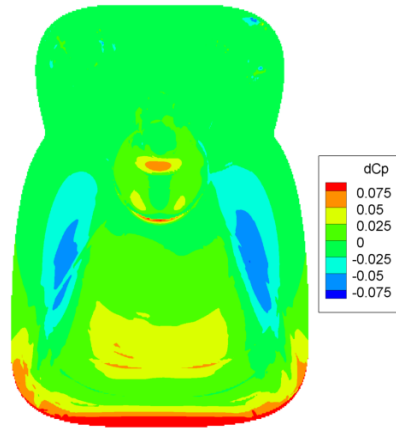
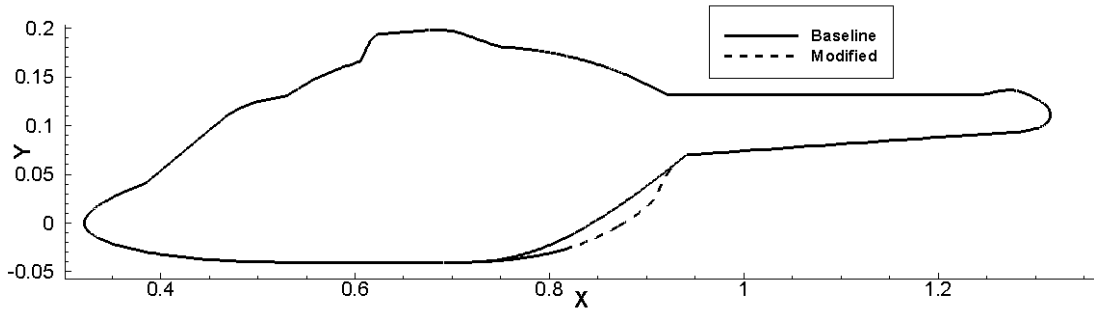


**Fig. 16.** Difference in pressure coefficient distribution between initial and optimized shapes including skirts at the rear fuselage.



(a)



(b)

**Fig. 17.** Comparison of modified baseline fuselages at the symmetry plane section (a), and fuselage layout with modified fuselage and landing fairing (b).

The results of the flow simulation around the fuselage with these additional modifications are presented in Table 4. It is shown that the total drag reduction is 4.6%. The drag decrease due to the fuselage modification only is 2.1%

**Table 4**

Drag coefficient of fuselage layout with different modifications.

Variant of layout	CD	$\Delta$ CD	$\Delta$ CD,%
Baseline geometry	0,1588	–	–
Modified fuselage and baseline landing skids	0,1555	0,0033	2,1
Modified fuselage and landing skids	0,1515	0,0040	4,6

The fuselage optimization considered free stream conditions without taking into account the main rotor influence. To simulate the flow around fuselage with rotor, an actuator disk model was used [37]. The actuator disk approximates the rotor using an infinitely thin source of momentum. This is modeled here as a steady, pressure jump across the disk. At the moment, the momentum source was modelled independently of the fuselage without any feedback between the two. For this reason, the effect of the rotor disk is simplified and the method, although computationally efficient, can only be used for initial estimates of the fuselage loads. To obtain the pressure jump for the mean rotor thrust, the uniform actuator disk was modeled using basic momentum theory. For a non-uniform disk a “typical” distribution of the pressure was estimated based on Heyson, Katzoff [38] and Shaidakov [39]. The distribution of the pressure jump across the disk surface is determined by the expression

$$\Delta p = \rho \gamma [\gamma \text{sign}(\delta)/2 + V_\infty \cos(\alpha - \alpha_a + \delta)]. \quad (4)$$

Here  $\delta$  is the angle of vortex cylinder slope,  $\alpha$  is the angle of attack of fuselage,  $\alpha_a$  is the angle of actuator incidence  $V_\infty$  is a free stream velocity,  $\rho$  is the air density. The function  $\gamma$  is distribution of circulation on the disk surface:

$$\gamma = \gamma_r + \gamma_s \sin(\psi), \quad (5)$$

where  $\psi$  is azimuth angle of considered point on disk surface.

The distribution of averaged blade load  $\gamma_r$  can be written in the form [39]

$$\gamma_r = C f_r(r_n), \quad (6)$$

where  $f_r(r_n) = r_n^2(2 - r_n^2 - r_n^4)$ ,  $r_n = r/R$  is normalized radius. The value of  $C$  is determined by the formula

$$C = 1.989V_\infty \left[ -\cos(\alpha - \alpha_a + \delta) + \sqrt{\cos^2(\alpha - \alpha_a + \delta) + 1.207 \frac{C_T}{\mu^2}} \right] \quad (7)$$

Here  $C_T=2T/(\rho\pi R^2 V_t^2)$  is the trust coefficient,  $\mu=V_\infty/V_t$  is the advanced ratio,  $V_t$  is the rotor tip velocity.

The expression for  $\gamma_s$  has the form

$$\gamma_s = CB\mu_v f_s(r_n), \quad (8)$$

where

$$B = \frac{8\mu_v(1+k_\delta^2)+a_\infty\sigma k_\delta}{(1+k_\delta^2)(4\mu_v+a_\infty\sigma k_\delta)}, \quad k_\delta = \tan\left(\frac{\pi}{4} - \frac{|\delta|}{2}\right), \quad f_s(r_n) = f_r(r_n)\left(r_n^{-1} - \frac{25}{13}r_n\right), \quad \mu_v = \mu\cos(\alpha - \alpha_a) + \frac{v_{xa}}{v_t}. \quad (9)$$

The expression for coefficient  $B$  contains the value  $a_\infty$  of the lift coefficient slope. The average value of the induced velocity  $v_{xa}$  is estimated using

$$v_{xa} = \text{sign}(\delta)k_\delta v_{1ya} \quad (10)$$

where

$$v_{1ya} = \frac{V_\infty}{2} \text{sign}(\delta) \left[ -\cos(\alpha - \alpha_a + \delta) + \sqrt{\cos^2(\alpha - \alpha_a + \delta) + \text{sign}(\delta) \frac{C_T}{\mu^2}} \right]. \quad (11)$$

In current work the non uniform pressure jump distribution is shown in Fig. 18. The pressure jump corresponds to the main rotor thrust coefficient of 0.01. This model allows to simulate the averaged influence of the main rotor on the fuselage aerodynamic characteristics [37]. In general a ‘‘real’’ main rotor has a more complex influence on the fuselage aerodynamics, due to the unsteady fuselage pressure distribution and flow asymmetry. Nevertheless the actuator disc model is widely used for approximate simulation of the main rotor effect at cruise flight conditions.

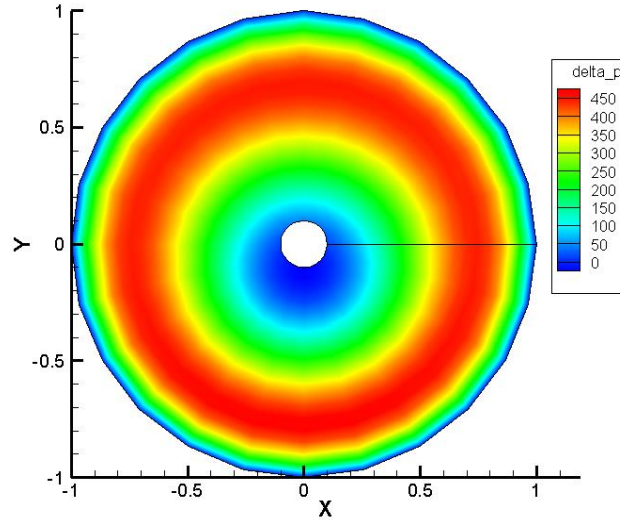


**Fig. 18.** Disc actuator pressure jump distribution (Free stream direction along the X axis).

The flow generated by the main rotor influences the vortex structure behind the helicopter fuselage (Fig. 19). In general, the rotor induced flow decrease the intensity of the vortex pair at the rear of the fuselage. The interaction between freestream and rotor induced flow depends on the helicopter flight speed. At low advance ratio ( $\mu=0.1$ ) the flow structure behind the fuselage is independent of the geometry modifications considered in the paper. At cruise conditions the main rotor influence on the fuselage is not significant, and the benefits of the modified geometry are present (Table 5).

**Table 5**

Drag coefficient of fuselage with main rotor.

Variant of fuselage	$\mu$	CD	$\Delta CD, \%$
Baseline	0.1	0,29	–
Modified fuselage	0.1	0,29	0
Baseline	0.15	0,1133	–
Modified fuselage	0.15	0,1124	0,8
Baseline	0.3	0,0909	–
Modified fuselage	0.3	0,0894	1,6

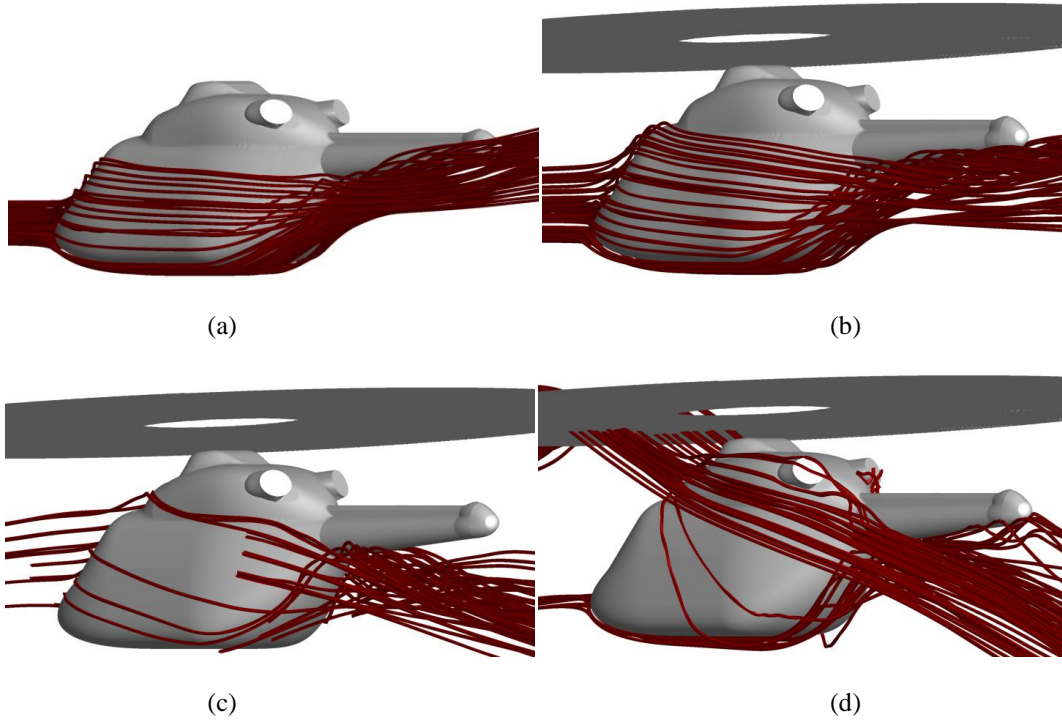


**Fig. 19.** Vortex structure behind the fuselage: isolated fuselage (a); advance ratio  $\mu=0.3$  (b); advance ratio  $\mu=0.15$  (c); advance ratio  $\mu=0.1$  (d).

## Conclusions

The paper presented optimization results of a realistic helicopter fuselage. The target function of the optimization process was the drag coefficient. Optimization of the cross section of the landing skids and the rear part of the fuselage were considered. The optimization was based on a Genetic Algorithm with Kriging as surrogate model.

As a result of the optimization of the landing skids, their geometry evolved to a symmetric aerofoil 38.8% thick. Investigation of the isolated fuselage drag showed a reduction up to 2.5% without compromising the functionality of the design. Application of the suggested modifications for a more complex fuselage layout (fuselage with skids and tail plain) gave a decrease of the drag coefficient by 4.6%. The benefits of the optimization were more pronounced for cases with the main rotor present at high advance ratios.

## Acknowledgments

This work was supported by the Ministry of Education and Science of the Russian Federation in the framework of project no. 9.1577.2017/PCh.

## References

- [1] J. Seddon, Aerodynamics of the Helicopter Rear Fuselage Upsweep, in: 8th European Rotorcraft Forum Proceedings, Aix-en-Provence, France, 1982.
- [2] R. Steijl, G. Barakos, CFD analysis of complete helicopter configurations – lessons learnt from the GOAHEAD project, *Aerospace Science and Technology*, Vol. 19, Issue 1, (June 2012), pp. 58-71.
- [3] W. Stalewski, J. Zoltak, Optimisation of the helicopter fuselage with simulation of main and tail rotor influence, in: 28th international congress of the aeronautical sciences (ICAS 2012), Brisbane, Australia, 2012.
- [4] C. Lienard, A. Le Pape, C. Verbeke, Numerical and Experimental Investigation of Helicopter Fuselage Drag Reduction Using Active Flow Control, in: American Helicopter Society 68th Annual Forum, Fort Worth, Texas, USA, May 1–3, 2012.
- [5] G. Gibertini, F. Auteri, G. Campanardi, G. Droandi, D. Grassi, A. Le Pape, A. Zanotti, Helicopter drag reduction by vortex generators, *Aerospace Science and Technology*, Vol. 47, (December 2015), pp. 324-339.
- [6] M. Wentrup, An Adjoint Based Gradient Optimization Chain For Complex Helicopter Fuselage Parts Using A Free Form Deformation Or Cad Based Parameterization Method, in: 41th European Rotorcraft Forum, Munich, Germany, September 1–4, 2015.

- [7] M. Grawunder, R. Reß, C. Breitsamter, Optimized Skid-Landing-Gears for Twin-Engine-Light Utility Helicopter. In: 39th European Rotorcraft Forum, Moscow, Russia, September 3–6, 2013, pp. 1-14.
- [8] M. Grawunder, R. Reß, C. Breitsamter, Helicopter Aft Body Drag Reduction by Passive Flow Control. In: 40th European Rotorcraft Forum, Southampton, UK, September 2–5, 2014, pp. 1-12.
- [9] C. Breitsamter, M. Grawunder, R. Reß, Aerodynamic Design Optimization for a Helicopter Configuration including a Rotating Rotor Head. In: 29th Congress of the International Council of the Aeronautical Sciences, St. Petersburg, Russia, September 7–12, 2014, pp.
- [10] A.S. Batrakov, A.N. Kusyumov, S.A. Mikhailov, V.V. Pakhov, A Study in Helicopter Fuselage Drag, in: 39th European Rotorcraft Forum, Moscow, Russia, September 3–6, 2013.
- [11] A.S. Batrakov, A.N. Kusyumov, S.A. Mikhailov, L.I. Garipova, G.N. Barakos, Vortical Flow Behind Isolated Helicopter Fuselage, in: 40th European Rotorcraft Forum, Southampton, UK, September 2-5, 2014.
- [12] A. Batrakov, L. Garipova, A. Kusyumov, S. Mikhailov, G. Barakos, Computational Fluid Dynamics Modeling of Helicopter Fuselage Drag, *Journal of Aircraft*, Vol. 52, No. 5 (2015), pp. 1634-1643.
- [13] A.N. Kusyumov, S.A. Mikhailov, A.O. Garipov, E.I. Nikolaev, G. Barakos, CFD simulation of fuselage aerodynamics of the «ANSAT» helicopter prototype, *Transaction on control and mechanical system*. Vol. 1, No. 7 (2012), pp. 318-324.
- [14] M. Biava, L. Vigevano, Simulation of a complete helicopter: A CFD approach to the study of interference effects, *Aerospace Science and Technology*, Vol. 19, Issue 1, (June 2012), pp. 37-49.
- [15] A. Kyrkos, J.A. Ekaterinaris, Assessment of an unstructured mesh approach for CFD predictions of the NH90 fuselage rotor, *Aerospace Science and Technology*, Vol. 19, Issue 1, (June 2012), pp. 77-85.
- [16] J.-C. Boniface, A computational Framework for Helicopter Fuselage Drag Reduction Using Vortex Generators, in: American Helicopter Society 70th Annual Forum, May 20-22, 2014 Montréal, Québec.
- [17] E. Ben-Hamou, E. Arad, A. Seifert, Generic Transport Aft-Body Drag Reduction using Active Flow Control, AIAA Paper 2004-2509, (2004).
- [18] N.W. Schaeffler, B.G. Allan, C. Lienard, and A. Le Pape, Progress Towards Fuselage Drag Reduction via Active Flow Control: A Combined CFD and Experimental Effort, in: 36th European Rotorcraft Forum Proceedings, Paris, France, September 7-9, 2010.
- [19] B.G. Allan, and N.W. Schaeffler, Numerical Investigation of Rotorcraft Fuselage Drag Reduction using Active Flow Control, in: American Helicopter Society 67th Annual Forum Proceedings, Virginia Beach, VA, May 3-5 2011.
- [20] G.T.K. Woo, A. Glezer, J. Bain, L. Sankar and T.M. Crittenden, Rotorcraft Fuselage Drag Reduction using Combustion Powered Actuators, AIAA Paper 2001-34, (2011).

- [21] S. Schneider, S. Mores, M. Edelmann, A. D'Alascio, D. Schimke, Drag Analysis for an Economic Helicopter, in: 37th European Rotorcraft Forum, September 13-15 2011, Vergiate/Gallarate, Italy.
- [22] R. Reiß, M. Grawunder and C. Breitsamter, Aerodynamic Analysis of a Helicopter Fuselage with Rotating Rotor Head, In: Progress in Flight Physics, EUCASS book series - Advances in Aerospace Sciences, 2015, ISBN 978-5-94588-165-5, pp. 99-110.
- [23] Q. Zhang, J.-D. Lee, J.-H. Wendisch, An adjoint-based optimization method for helicopter fuselage backdoor geometry, in: 36th European Rotorcraft Forum 2010, 7.-9. Sep. 2010, Paris, Frankreich.
- [24] Q. Zhang, A. Garavello, A. D'Alascio, D. Schimke, Advanced CFD-based Optimization Method Applied to the Industrial Design Process of Airframe Components at Airbus Helicopters, in: American Helicopter Society 70th Annual Forum, May 20-22, 2014 Montréal, Québec.
- [25] G. Bohling, <http://people.ku.edu/~gbohling/cpe940/Kriging.pdf>.
- [26] J. Mc Call, Genetic algorithm for modeling and optimization, Journal of Computational and Applied Mathematics, Vol. 184, Issue 1 (2005), pp. 205-222.
- [27] C. Kim, Computational Elements for High-fidelity Aerodynamic Analysis and Design Optimisation, Defence Science Journal, Vol. 60, No. 6, November 2010, pp. 628-638.
- [28] C.S. Johnson and G.N. Barakos, Optimising Aspects of Rotor Blades in Forward Flight, in: 49th AIAA Aerospace Sciences Meeting including the New Horizons Forum and Aerospace Exposition, January 4 – 7, 2011, Orlando, Florida.
- [29] G. Barakos, R. Steijl, K. Badcock, A. Brocklehurst, Development of CFD Capability for Full Helicopter Engineering Analysis, in: Proceedings of the 31st European Rotorcraft Forum, 13-15 September, 2005, Florence, Italy.
- [30] P. Spalart, S. Allmaras, A one-equation turbulence model for aerodynamic flows, American Institute of Aeronautics and Astronautics, 1992. AIAA-92-0439, Technical Report.
- [31] D. C. Wilcox, Turbulence modeling for CFD, La Canada, California: DCW Industries, Inc., 1994.
- [32] F. R. Menter, Zonal two equation  $k-\omega$  turbulence models for aerodynamic Flows, AIAA Paper, №93-2906 (1993), pp. 1-21.
- [33] L. Davidson, The SAS model: a turbulence model with controlled modelled dissipation, in: 20th Nordic seminar on computational mechanics, 2007, 20-23 Nov., Göteborg.
- [34] A. A. Giunta, Jr. S. F. Wojtkiewicz, M. S. Eldred, Overview of modern design of experiments methods for computational simulations, AIAA paper, 2003-0649.
- [35] J. D. Berry, S. L. Althoff, Computing induced velocity perturbations due to a helicopter fuselage in a freestream, NASA Technical Memorandum 4113, TR 89-B-001, 1989.

- [36] E.M. Zakharov, I.K. Manishina, Review of multidimensional optimization methods, in: Mathematical models, numerical methods, information processes, Value 14 №3 (2014), pp. 256-274 [In Russian].
- [37] A.S. Batrakov, A.N. Kusyumov, G. Barakos, Simulation of flow around fuselage of helicopter using actuator disc theory, in: 29th Congress of the International Council of the Aeronautical Sciences, 7-12 September, 2014, St. Petersburg, Russian Federation, pp. 1-7.
- [38] H. Heyson, S. Katzoff, Induced velocities near a lifting rotor with nonuniform disk loading, NACA-TR-1319, 1957.
- [39] V.I. Shaidakov, Helicopter design, in: Proceedings of Moscow Aviation Institute, Vol. 31(1978) 68 p. [in Russian]